Electronic Supplementary Material (ESI) for Energy & Environmental Science.
This journal is © The Royal Society of Chemistry 2021

Electronic Supplementary Information (ESI†)

Towards high-areal-capacity aqueous zinc-manganese batteries: promoting MnO_2 dissolution by redox mediators

*Jiafeng Lei, Yanxin Yao, Zengyue Wang and Yi-Chun Lu**

Electrochemical Energy and Interfaces Laboratory
Department of Mechanical and Automation Engineering
The Chinese University of Hong Kong
Shatin, N. T. 999077, Hong Kong SAR, China
*E-mail: yichunlu@mae.cuhk.edu.hk

Experimental section

Chemicals and materials: Zinc acetate ($Zn(CH_3COO)_2$, 99%), manganese acetate tetrahydrate ($Mn(CH_3COO)_2{\cdot}4H_2O$, 99%), and potassium chloride (KCl, 99%) were all received from Aladdin, Shanghai. Manganese dioxide (MnO_2, 99%) was received from Meryer. Potassium iodide (KI, ≥99%) was received from Sigma-Aldrich. All chemicals were used as received without further purification.

Static Cell assembly: Carbon felt with a thickness of 5 mm was used as both cathode and anode without any modification. In the $Zn\text{-}Mn^{2+}/MnO_2$ static cell, a homemade cell was constructed by using carbon felt as the cathode-less current collector on the cathode side, glass fiber as the separator and the carbon felt with a zinc plate (0.1 mm) as the anode. The carbon felt was pressed to 3 mm in the cell. The geometric area of the electrode for the static cell is 2 cm^2 (diameter 16 mm) for both positive and negative electrodes. 500 μL electrolyte was added at both positive side and negative side respectively with the composition of 1 M $Zn(Ac)_2$ + 1 M $Mn(Ac)_2$ + 2 M KCl with or without 0.1 M KI. 1 M $Zn(Ac)_2$ + 1 M $Mn(Ac)_2$ + 2 M KCl with 0.05 M or 0.5 M KI is studied for mediator concentration effect. For the pure Zn-KI static cell, the electrolyte composition is 1 M $Zn(Ac)_2$ + 2 M KCl with 0.05 M, 0.1 M, and 0.5 M KI. For the static cells shown in Fig. S8, two carbon felts with the geometric area of 2 cm^2 were stacked and pressed to 6mm with 1 mL electrolyte added at both positive side and negative side (2 mL electrolyte in total).

Flow Cell assembly: For the $Zn\text{-}Mn^{2+}/MnO_2$ flow cell, the cathode and anode are all commercial SGL carbon felt without modification and a Nafion® membrane (N117) was applied to avoid water crossover. Before the usage, the Nafion 117 was firstly treated with H_2O_2 under 80 ℃ for 1h to remove the impurities, followed by soaked in 5% H_2SO_4 under 80 ℃ for 1 h. Then, the H^+ type Nafion 117 was treated by 1 M KOH under 80 ℃ for 2 h, converting to K^+ type cation exchange membrane. The membrane then was washed by deionized (DI) water and soaked in DI water overnight before usage. A small piece of zinc plate (0.1 mm) was placed in anode side and the flow field is serpentine type. The effective geometric electrode area for the flow cell is 4 cm^2 (2 cm × 2 cm) for both positive and negative electrodes. The carbon felt was pressed to 3 mm which is the thickness of the PTFE frame during operation. The electrolyte composition is 1 M $Zn(Ac)_2$ + 1 M $Mn(Ac)_2$ + 2 M KCl with or without 0.1 M KI, in which the volume is 10 mL for both positive side and negative side respectively. We select acetate ions because it was reported to effectively improve the battery cycling stability[1, 2]. 2 M KCl is added to increase the electrolyte conductivity (Fig. S20, ESI†). For the flow cell tests with areal capacity higher than 40 mAh cm^{-2}, large osmotic pressure was observed due to the reduced ion concentration in the positive electrode side. Therefore, an additional 2 M KCl was added into the posolyte of the flow cells (1 M $Mn(Ac)_2$ + 1 M $Zn(Ac)_2$ + 4 M KCl) to maintain the osmotic pressure when cycling at areal capacity higher than 40 mAh cm^{-2}. After certain cycles under high areal capacity, the carbon felt on the anode side was changed with a new one to eliminate the dendrite effects, which are all indicated in the figures. A peristaltic pump was used to drive the electrolyte and the flow rate for the posolyte and negolyte is approximately 40 mL min^{-1}.

Material characterization: The UV-visible (UV-vis) spectra were collected by SEC2000 UV-visible Spectrophotometer (ALS Co., Ltd.). For the solution in the UV-vis test, 1 M HAc was added as the supporting electrolyte to support enough protons. An SCE-C thin layer quartz glass cell with an optical path length of 1 mm was used as the electrolyte holder and the solution was diluted for 100 times for each test. The scanning electron microscopy (SEM) was conducted by Quanta 400F scanning electron microscope (FEI) with an accelerating voltage of 10 kV. The SEM was employed to detect the electrode morphology with or without KI. The samples in Fig. 4 were soaked in DI water for 3 times to remove the soluble salts and then tried in vacuum before the SEM test. X-ray diffraction (XRD) was performed on a Rigaku Smart Lab diffractometer (Cu Kα radiation). The membranes were washed by DI water for 3 times to remove the soluble salts then dried in room temperature before the XRD test.

Electrochemical measurements: The cyclic voltammetry (CV) tests on manganese species and iodide were conducted in a three-electrode system using the carbon paper as the working electrode, the zinc plate as the counter electrode and a saturated-calomel electrode (SCE) as the reference electrode by a VMP3 electrochemical testing unit (Bio-Logic, France). The scanning rate is 10 mV s^{-1} and the electrolyte volume is 10 mL with 1 M $Zn(Ac)_2$ as the supporting electrolyte. The linear sweep voltammetry (LSV) was conducted in the same electrode with CV tests and 1 M $Zn(Ac)_2$ + 1 M $Mn(Ac)_2$ electrolyte was tested to find out the stable operating window. The 1 M $Zn(Ac)_2$ electrolyte without $Mn(Ac)_2$ was also tested as the background to exclude the manganese effect on the oxygen evolution reaction. The scanning rate is 1 mV s^{-1}. In the H-cell test, a Nafion 117 membrane was applied as the separator and 1 M KCl was applied as supporting electrolyte with a zinc plate as the negative electrode and the carbon paper as the positive electrode. 1 M HAc was added at the positive side to support enough protons. The galvanostatic charging was performed on LAND Battery Testing System (Land, Wuhan Land Electronic Co., Ltd.). The battery was determined by limited capacity for the charging process and a cut-off voltage of 0.2 V was applied for the discharging process.

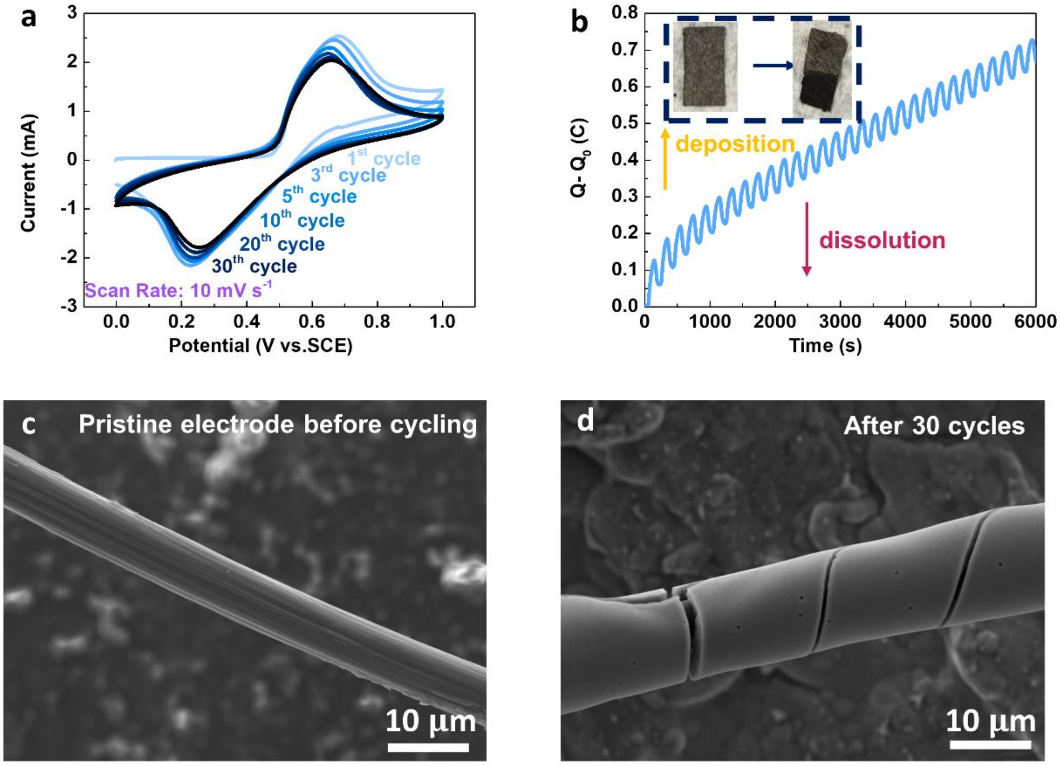

Figure S1. (a) CV curves for 50 mM Mn(Ac)$_2$ on the carbon paper electrode at 1st, 3rd, 5th, 10th, 20th, 30th cycles in 1 M Zn(Ac)$_2$ at 10 mV s^{-1}; (b) Charge-time profile for the electrode shows the accumulation of charge due to incomplete dissolution and the inset shows some black solids on the electrode after cycling; (c-d) The SEM images of the electrode before and after CV cycling.

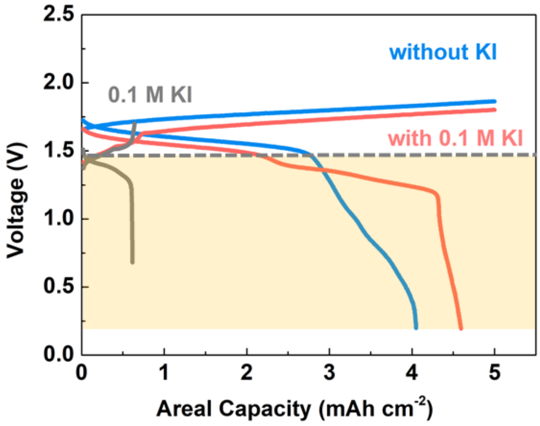

Figure S2. The voltage-capacity profiles of the Zn-Mn^{2+}/MnO_2 cells at the 10th cycle with a pure Zn-KI cell as a background comparison under 10 mA cm^{-2}. The potential range for I^-/I_3^- is the potential below than 1.45 V and the capacity from iodide is ~ 0.6 mAh cm^{-2}.

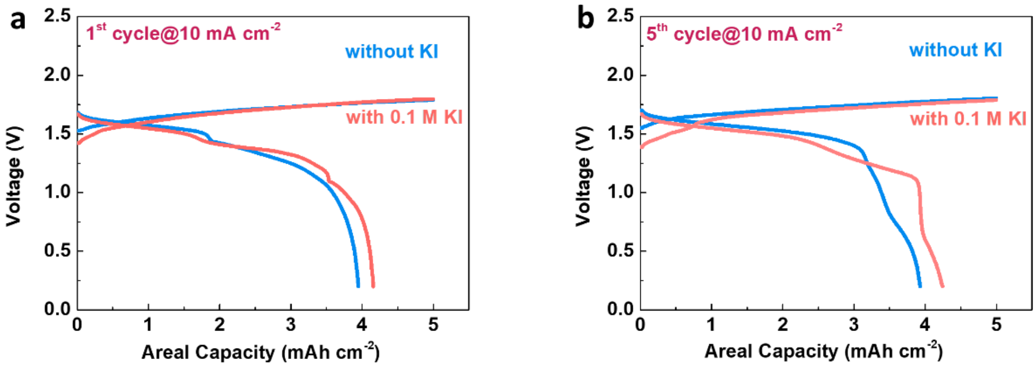

Figure S3. The voltage-capacity profiles of the Zn-Mn^{2+}/MnO_2 cell with or without KI at the (a) 1st and (b) 5th cycle under 10 mA cm^{-2}. The increased potential for the Zn-Mn^{2+}/MnO_2 cell without KI is ascribed to the consumption of Mn^{2+} and the accumulation of protons according to the Nernst equation:

$$Mn(Ac)_2 + 2H_2O \Leftrightarrow MnO_2 + 2HAc + 2H^+ + 2e^-$$

$$E = E^0 + \frac{RT}{2F} * \ln\frac{[a(H^+)^2 * a(HAc)^2]}{a(Mn(Ac)_2)^1}$$

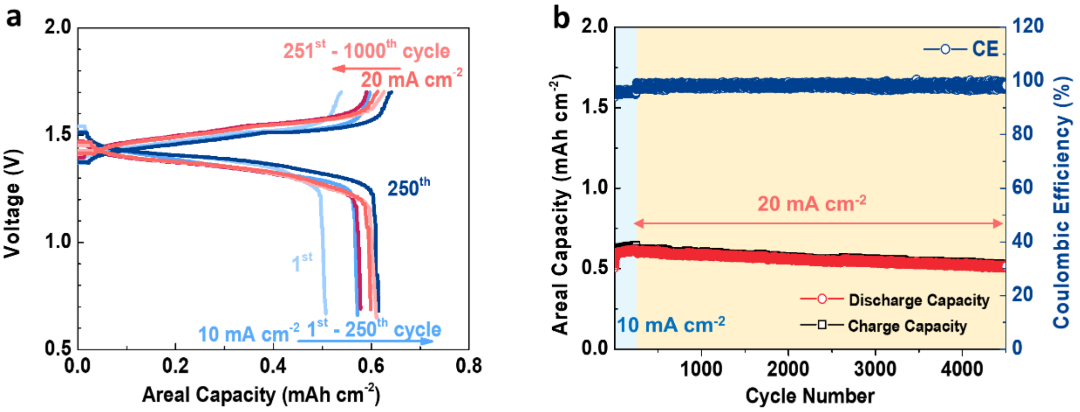

Figure S4. The cycling performance of the pure Zn-KI cell with 0.1 M KI in 1 M $Zn(Ac)_2$ electrolyte under 10 mA cm^{-2} for 250 cycles and 20 mA cm^{-2} for the following 4250 cycles.

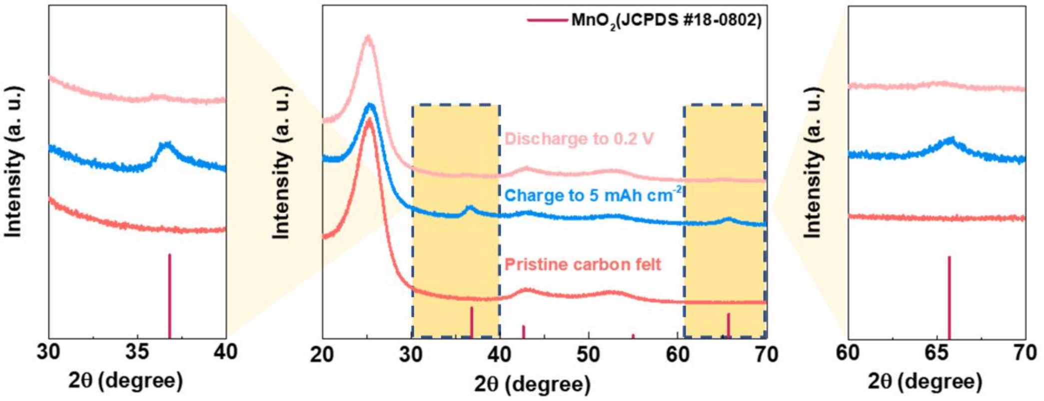

Figure S5. The XRD patterns of the pristine carbon felt electrode and the carbon felt electrode (positive electrode) in the Zn-Mn^{2+}/MnO_2 cell with 0.1 M KI upon charge to 5 mAh cm^{-2} and discharge to 0.2 V.

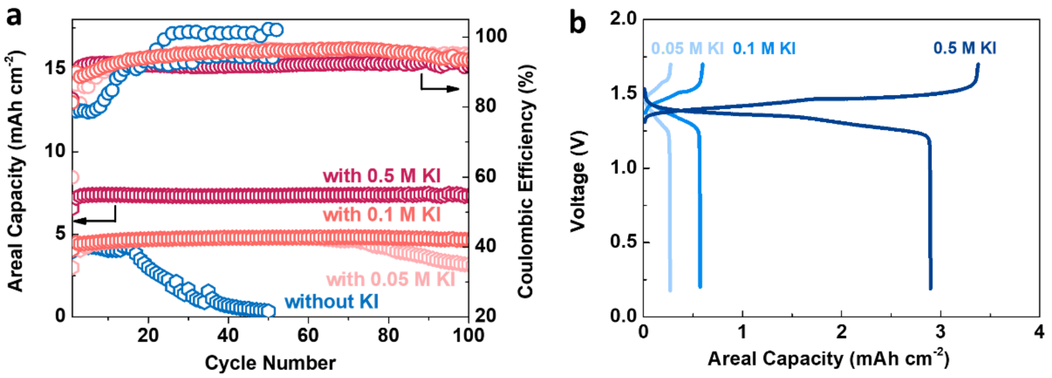

Figure S6. (a) The cycling performance and CE of the Zn-Mn^{2+}/MnO_2 cell with 0.05 M, 0.1 M and 0.5 M KI. The Zn-Mn^{2+}/MnO_2 cell with 0.05 M and 0.1 M KI are cycled in 5 mAh cm^{-2} and Zn-Mn^{2+}/MnO_2 cell with 0.5 M KI cycled in 8 mAh cm^{-2} to account for the capacity contributed from 0.5 M KI of around 3 mAh cm^{-2} for fairness. (b) The voltage-capacity profiles of the Zn-I cell with 0.05 M, 0.1 M and 0.5 M KI. The areal capacity contributed from 0.5 M KI is around 3 mAh cm^{-2}.

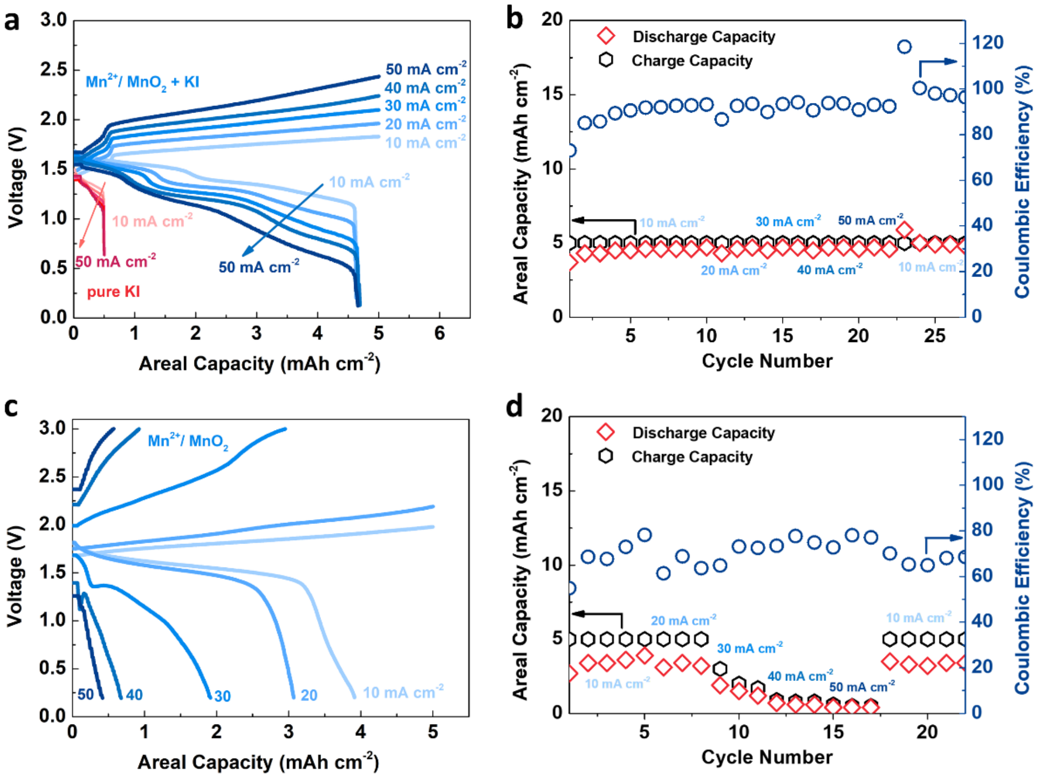

Figure S7. (a) Galvanostatic voltage profiles (blue lines) and (b) CE-capacity retention of the Zn-Mn^{2+}/MnO_2 cell with 0.1 M KI at various rates. The discharge profiles of a pure Zn-0.1M KI cell are included in (a) with red lines from 10 mA cm^{-2} to 50 mA cm^{-2}. (c) Galvanostatic voltage profiles and (d) CE-capacity retention of the Zn-Mn^{2+}/MnO_2 cell without 0.1 M KI at various rates. The charge cut-off condition for all Zn-Mn^{2+}/MnO_2 cells was 5 mAh cm^{-2} or reaching 3 V.

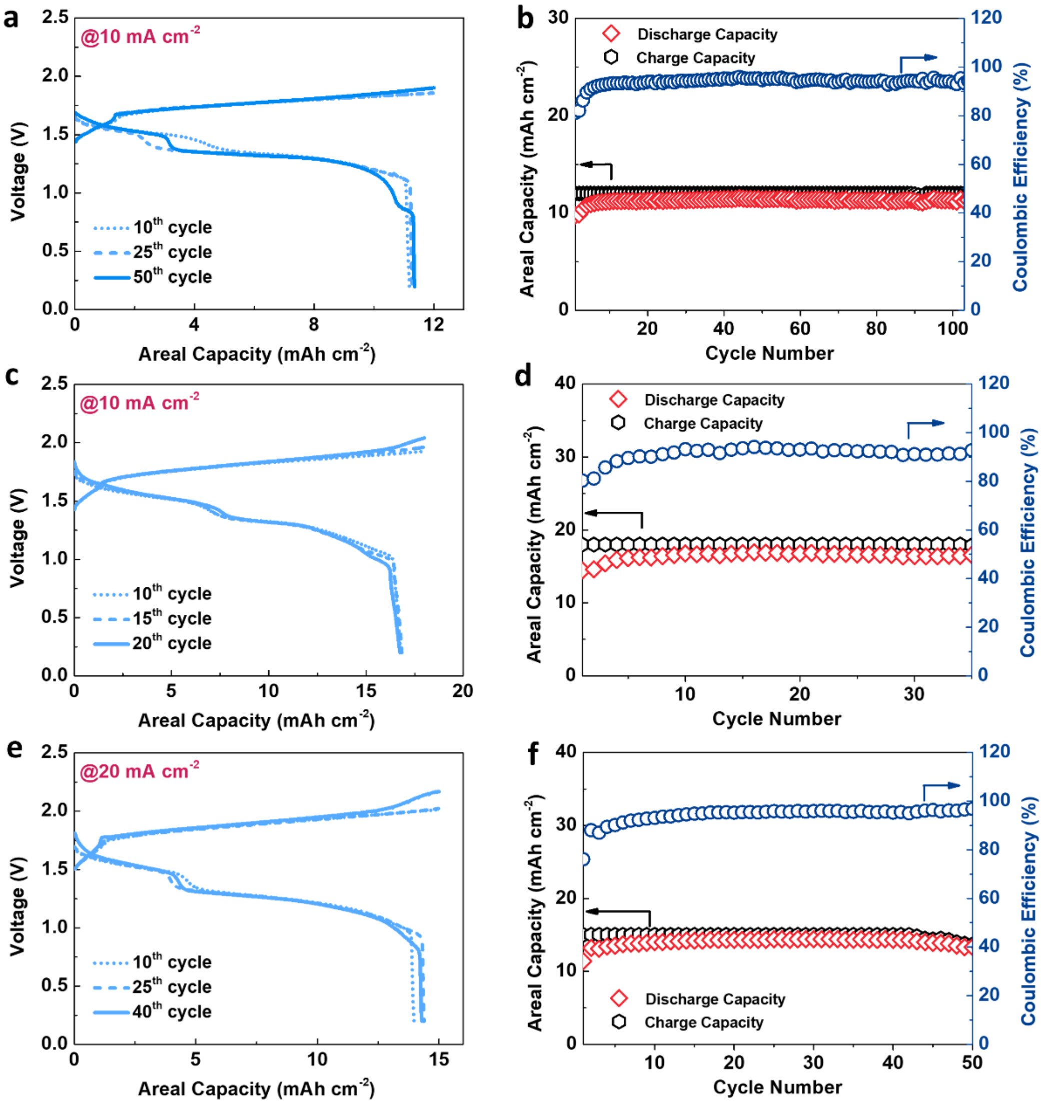

Figure S8. The voltage profiles and the cycling stability of the Zn-Mn^{2+}/MnO_2 cell with 0.1 M KI at (a)(b) 10 mAh cm^{-2} and (c)(d) 18 mAh cm^{-2} under 10 mA cm^{-2} and (e)(f) 15 mAh cm^{-2} under 20 mA cm^{-2}. Two carbon felts with the area of 2 cm^2 are stacked and pressed to 6 mm with 1 mL electrolyte added at both positive side and negative side respectively (2 mL electrolyte in total).

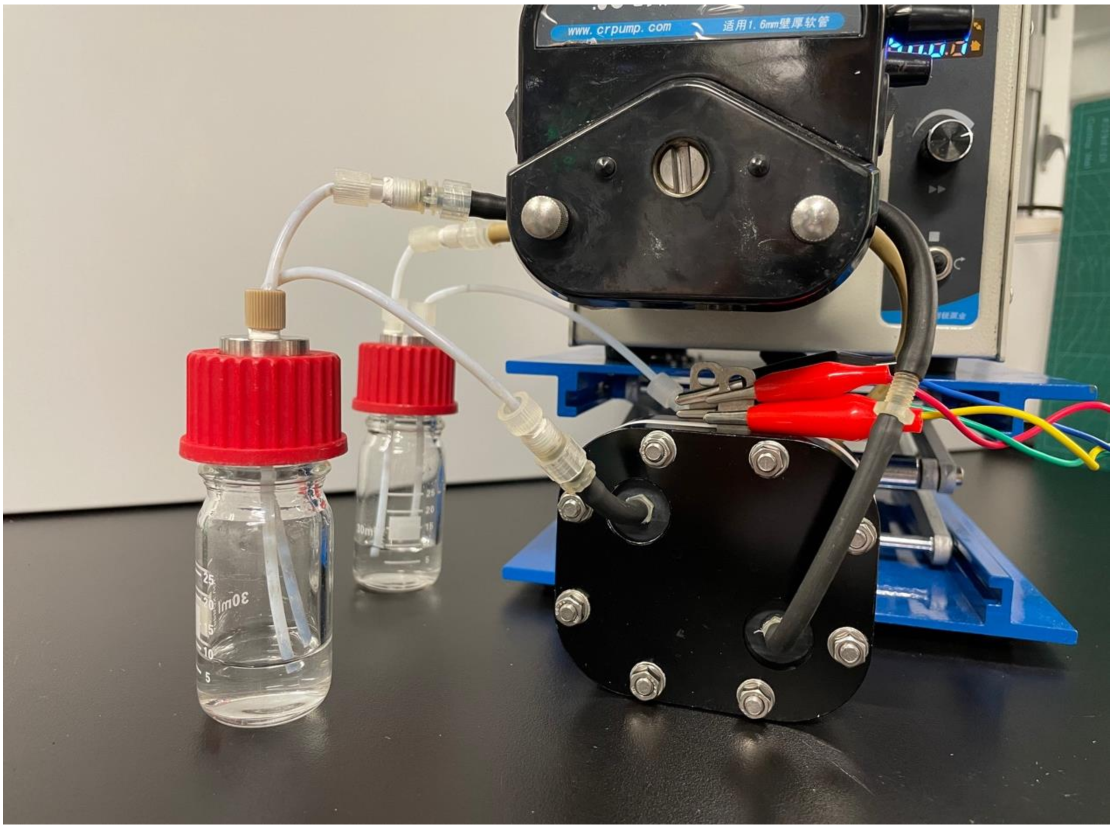

Figure S9. The optical image of the flow cell.

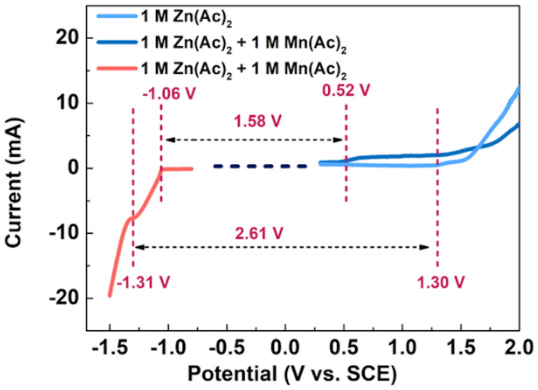

Figure S10. The operating window analysis of the electrolyte in a three-electrode system with the carbon paper as the working electrode, the zinc plate as the counter electrode and a saturated calomel electrode (SCE) as the reference electrode. The scanning rate is 1 mV s^{-1}. To eliminate the influence of $Mn(Ac)_2$ on the oxygen evolution reaction, 1 M $Zn(Ac)_2$ electrolyte without $Mn(Ac)_2$ was also tested as the background.

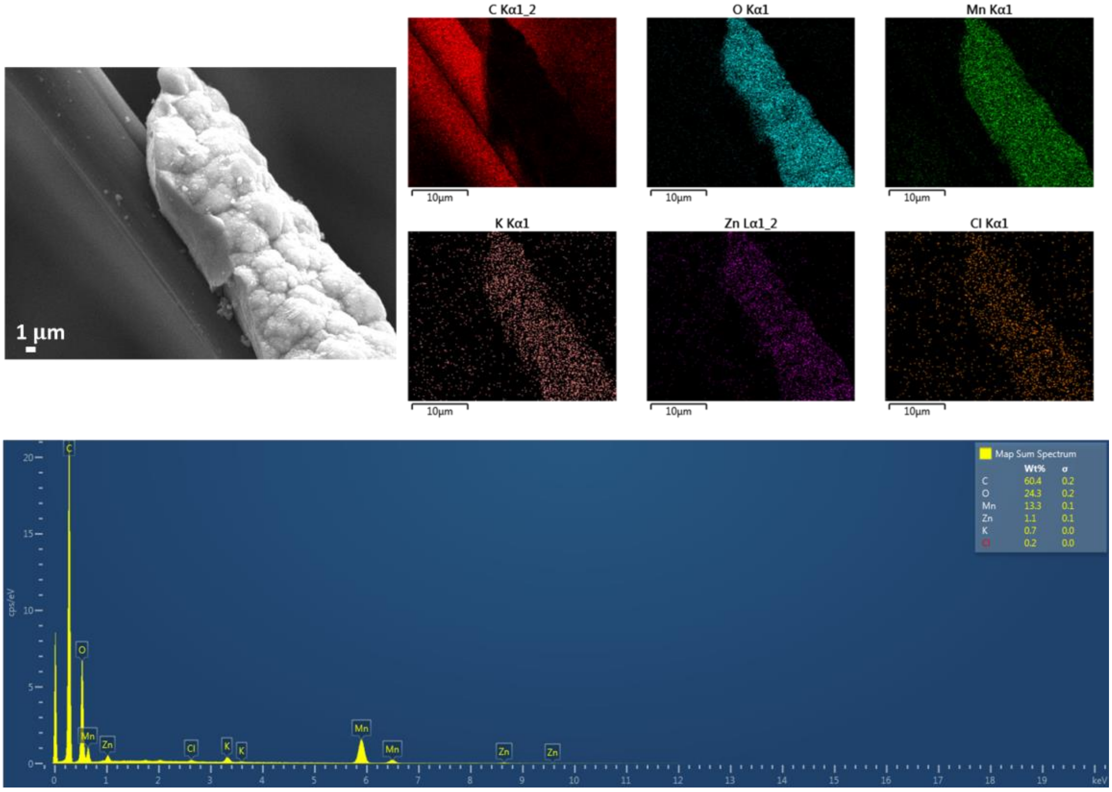

	Wt%	σ
C	60.4	0.2
O	24.3	0.2
Mn	13.3	0.1
Zn	1.1	0.1
K	0.7	0.0
Cl	0.2	0.0

Figure S11. The EDS mapping of the residual MnO_2 on the electrode from the Zn-Mn^{2+}/MnO_2 cell without KI. The element of K, Zn, Cl may come from the absorbed salt on the carbon felt or the side reactions such as cation insertion reaction[3].

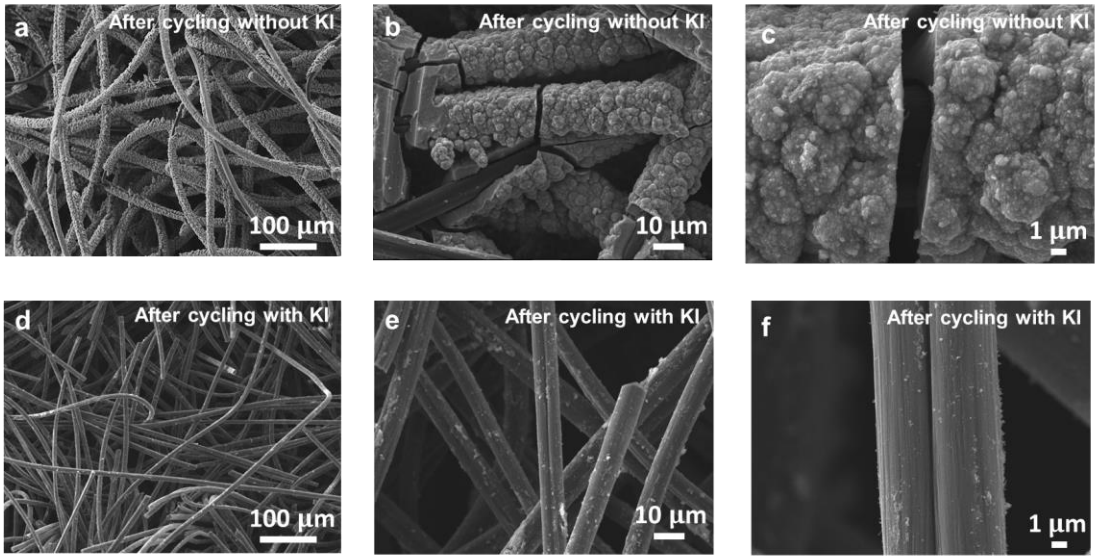

Figure S12. The SEM images of the electrode after cycling (a-c) without and (d-f) with KI after 25 cycles under 20 mA cm^{-2}. The areal capacities are (a-c) 15 mAh cm^{-2} and (d-f) 20 mAh cm^{-2}.

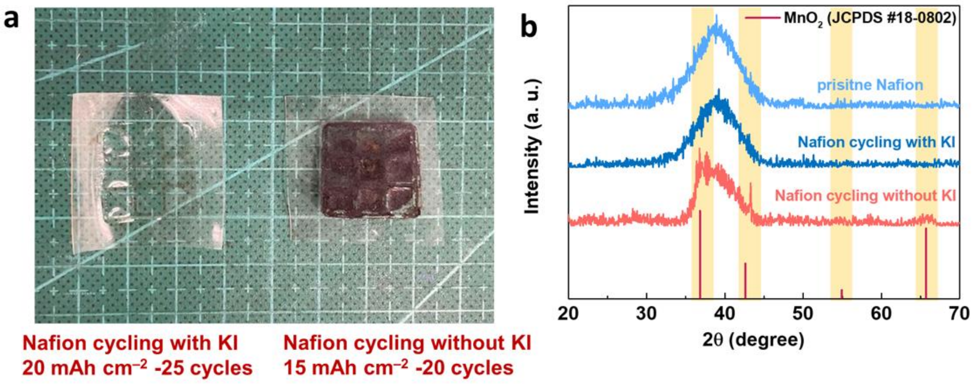

Figure S13. (a) The optical images of the membrane without KI (right) under 15 mAh cm^{-2} for 20 cycles and the transparent membrane with KI (left) under 20 mAh cm^{-2} for 25 cycles; (b) The XRD characterizations of the pristine membrane and the membrane with or without KI after cycling.

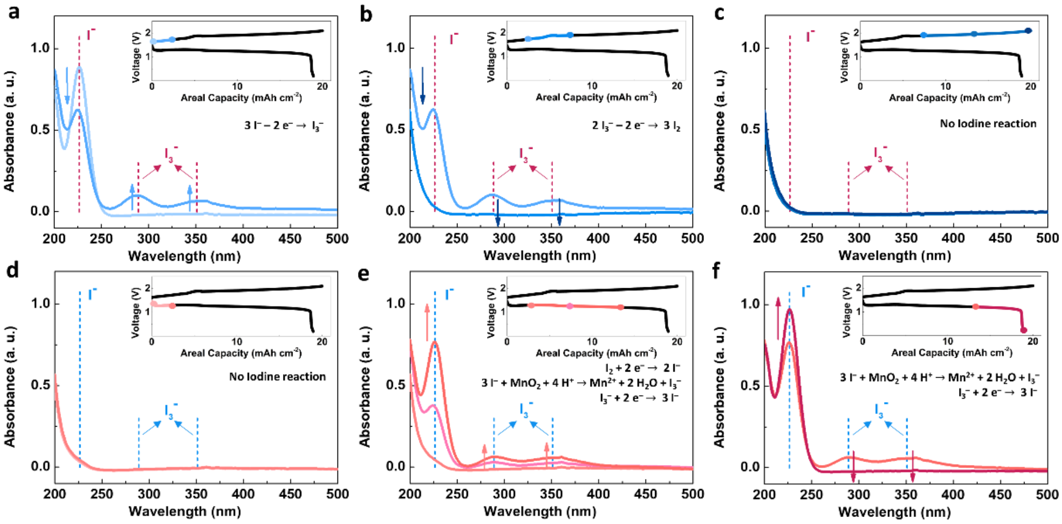

Figure S14. The UV-vis spectrum of the Zn-Mn^{2+}/MnO_2 cell with 0.1 M KI at 20 mAh cm^{-2} in flow mode during charge and discharge processes. (a) Charge from 0 mAh cm^{-2} to 2.5 mAh cm^{-2}; (b) charge from 2.5 mAh cm^{-2} to 7.5 mAh cm^{-2}; (c) charge from 7.5 mAh cm^{-2} to 19.5 mAh cm^{-2}; (d) discharge from 0 mAh cm^{-2} to 2.5 mAh cm^{-2}; (e) discharge from 2.5 mAh cm^{-2} to 13.5 mAh cm^{-2}; (f) discharge at the end of the discharge.

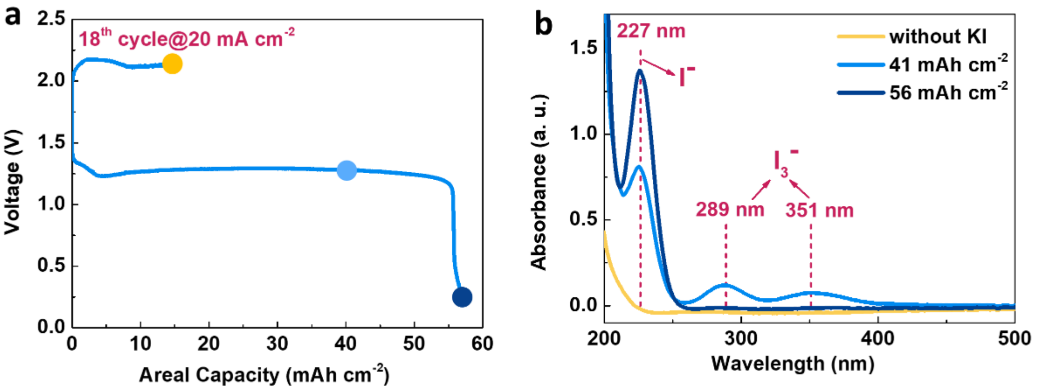

Figure S15. (a) The charge/discharge profile at the 18th cycle. In the 18th cycle, 0.1 M KI was added after charged and the discharging profile in the 18th cycle shows the capacity recovery with 57 mAh cm^{-2} released while only 15 mAh cm^{-2} was charged in this cycle; (b) The UV-vis spectrum analysis during the discharging process in the 18th cycle. The presence of I_3^- during discharging process verifies the mediator reaction as only I^- in the reduced form was added. The electrolyte composition is 1 M $Mn(Ac)_2$ + 1 M $Zn(Ac)_2$ + 2 M KCl (+ 0.1 M KI).

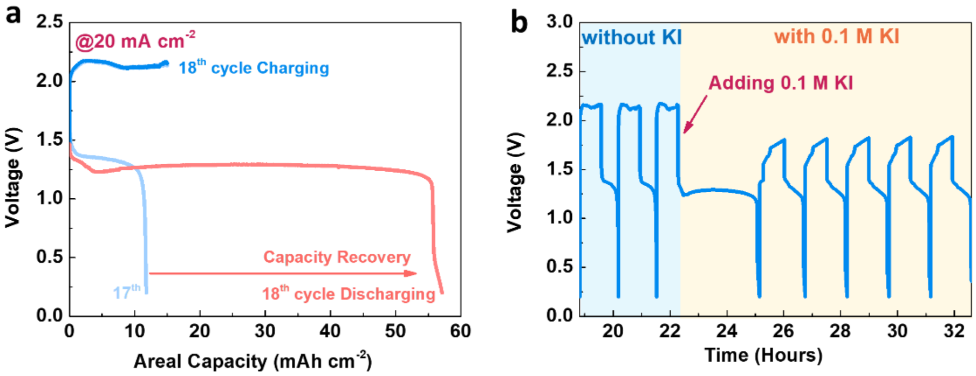

Figure S16. (a) The charge/discharge profiles in the 17th and 18th cycle. In the 18th cycle, 0.1 M KI was added after charged and the 18th charging profile overlays with the 17th charging profile. The discharging profile in the 18th cycle shows the capacity recovery with 57 mAh cm^{-2} released while only 15 mAh cm^{-2} was charged in this cycle; (b) The time-voltage profile of the cell from the 15th cycle to the 23rd cycle under 15 mAh cm^{-2}. The electrolyte composition is 1 M $Mn(Ac)_2$ +1 M $Zn(Ac)_2$ + 2 M KCl (+ 0.1 M KI).

18th cycle charged state

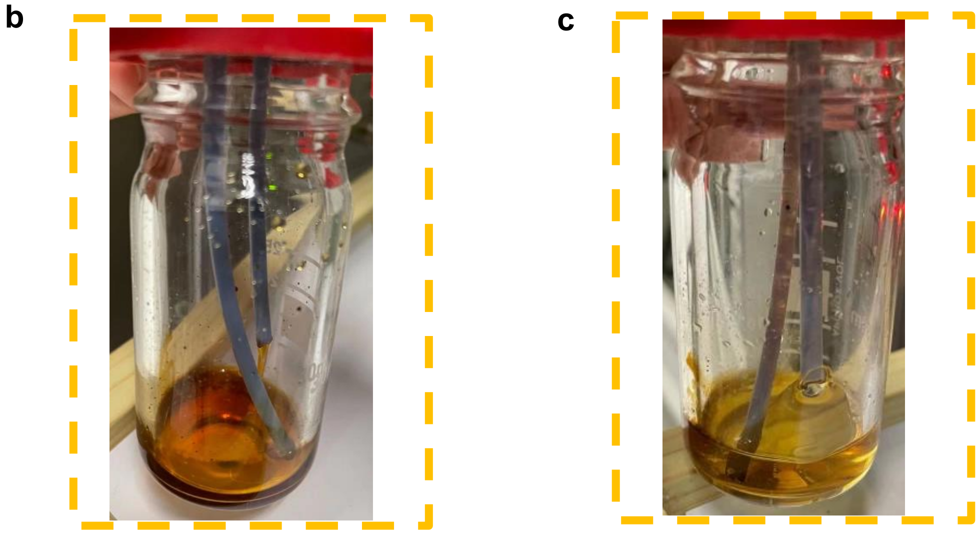

After Adding KI

18th cycle discharged state

Figure S17. (a) The optical images of the solution in tank before adding KI; The optical images of the solution in tank (b) after adding KI and (c) after discharging.

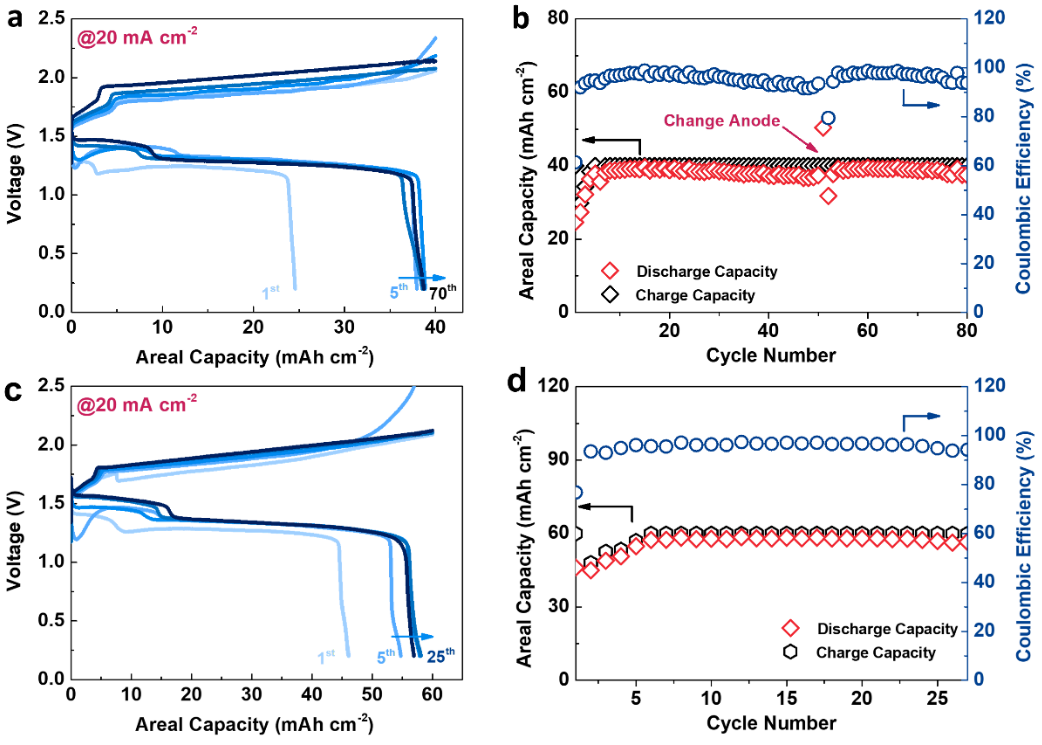

Figure S18. The (a) voltage profiles and the (b) cycling performance of the Zn-Mn^{2+}/MnO$_2$ cell with 0.1 M KI at 40 mAh cm^{-2} under 20 mA cm^{-2} (over 13 days); The (c) voltage profiles and the (d) cycling performance of the Zn-Mn^{2+}/MnO$_2$ cell with 0.1 M KI at 60 mAh cm^{-2} under 20 mA cm^{-2}.

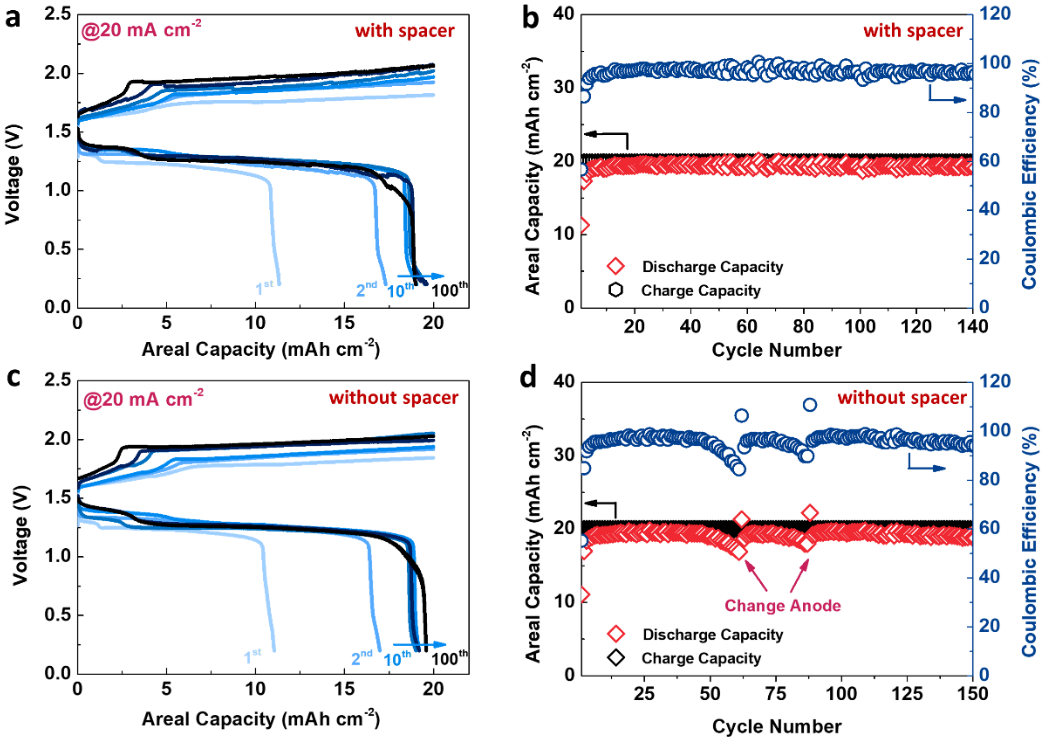

Figure S19. The voltage profiles and the cycling stability of the Zn-Mn^{2+}/MnO$_2$ cell with 0.1 M KI at 20 mAh cm^{-2} under 20 mA cm^{-2} (a-b) with or (c-d) without a 1 mm spacer.

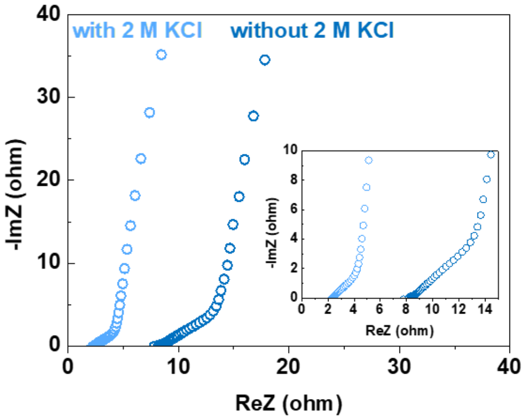

Figure S20. The EIS results of the Zn-Mn^{2+}/MnO_2 cells using 1 M $Zn(Ac)_2$ + 1 M $Mn(Ac)_2$ (dark blue) or 1 M $Zn(Ac)_2$ + 1 M $Mn(Ac)_2$ + 2 M KCl (light blue).

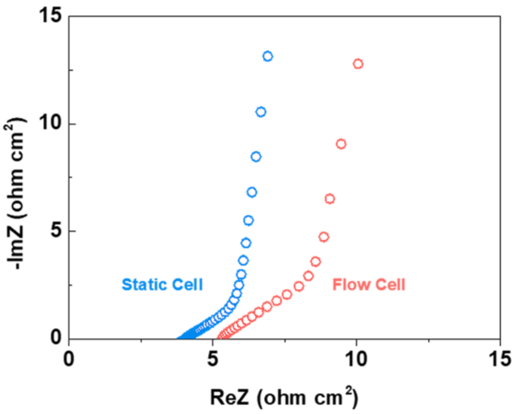

Figure S21. The EIS results of the Zn-Mn^{2+}/MnO$_2$ cells with 2 M KCl and 0.1 M KI in static cell with electrode area of 2 cm^2 and flow cell with electrode area of 4 cm^2.

Table S1. The comparison of areal capacity for Mn^{2+}/MnO_2 -based batteries.

Battery Type	Areal Capacity (mAh cm^{-2})	Cycle Number[a]	Voltage (V)	Electrode Area (cm ^{2})	Electrolyte Volume	Capacity per cell (mAh)	Volumetric energy density[b, c] (Wh L^{-1})	Electrolyte Composition	Ref.
H-Mn	1	10000	1.4	unknown	unknown	unknown	unknown	1 M $MnSO_4$ + 0.05 M H_2SO_4	[4]
	1.5	1400		10	14 mL	15	1.5		
	4	600		1	0.2 mL	4	28		
	6	40				6	42		
Cu-Mn	0.8	2000	1	unknown	unknown	unknown	unknown	0.3 M $MnSO_4$ + 0.3 M $CuSO_4$ + 0.5 M H_2SO_4	[5]
	3.2	50							
Zn-Mn	0.8	1000	2	unknown	unknown	unknown	unknown	0.3 M $MnSO_4$ + 0.3 M $ZnSO_4$	
Bi-Mn	0.8	200	1.1	unknown	unknown	unknown	unknown	0.1 M $MnSO_4$ + 0.1 M $Bi(NO_3)_2$ + 1 M HNO_3	
Cu-Mn	8.3	50	1.1	30*4=120	155 mL	1000	7	0.8 M $MnSO_4$ +0.8 M $CuSO_4$ + 0.5 M H_2SO_4	[6]
	10	1	1.1	unknown	unknown	unknown	unknown		
	51.7	1	1.1	30*4=120	155 mL	6285	44.6		
Pb-Mn	5	80	1.65	20	10 mL	100	16.5	1 M $MnSO_4$ + 0.5 M H_2SO_4	[7]
	5	500	1.65	20	150 mL	100	1.1	1 M $MnSO_4$ + 0.5 M H_2SO_4	
Zn-Mn	2	1800	1.95	9	1 ml	18	36	1 M $MnSO_4$ + 1 M $ZnSO_4$ + 0.1 M H_2SO_4	[3]
	10	1		unknown	unknown	unknown	unknown		
Zn-Mn	1	450	2.5	2	0.5 mL	2	10	3 M $MnSO_4$ + 0.3 M H_2SO_4 + 0.06 M $NiSO_4$ $\Vert$ 3 M NaOH + 0.3 M ZnO	[8]
Zn-Mn	15.5	1	2.45	1.25	unknown	19.4	unknown	1 M $MnSO_4$ + 0.5 M H_2SO_4 $\Vert$ 0.1 M $Zn(Ac)_2$ + 2.4 M KOH	[9]
	0.4	1500				0.5	unknown		
	0.4	6000	2.45			0.5	unknown		

Zn-Mn	0.5	4000	1.6	0.5	unknown	0.25	unknown	0.4 M $Mn(Ac)_2$ + 1 M $Zn(Ac)_2$	[1]
	1	1000				0.5	unknown		
	2	225				1	unknown		
Zn-Mn	7	400	1.6	48	50 mL	336	10.7	0.5 M $Mn(Ac)_2$ + 0.5 M $ZnCl_2$ + 2 M KCl	[2]
	13.3	100				638.4	20.4	0.5 M $Mn(Ac)_2$ + 0.5 M $Zn(Ac)_2$ + 2 M KCl	
	16.7	50		9	5 mL	150	48	1M $Mn(Ac)_2$ + 1 M $Zn(Ac)_2$ + 2 M KCl	
	20	30		48	50 mL	960	30.7	1.5 M $Mn(Ac)_2$ +1.5 M $ZnCl_2$+ 3 M KCl	
Zn-Mn	0.15	11000	1.7	unknown	unknown	unknown	unknown	0.2 M $MnSO_4$ + 2 M $ZnSO_4$	[10]
	1	80							
Zn-Mn	2.2	500	1.9	50*10=500	0.52 L	1100	4	1 M $MnSO_4$ + 1 M $ZnSO_4$	[11]
Zn-Mn	2.5	400	1.6	2	0.5 mL	5	16	1 M $Mn(Ac)_2$ + 1 M $Zn(Ac)_2$ + 2 M KCl + 0.1 M KI	This Work
	5	100				10	32		
	12	100			1 mL	24	38.4		
	15	50				30	48		
	18	30				36	57.6		
	15	225 [d]		4	10 mL	60	9.6		
	20	140				80	12.8		
	40	80[d]				160	25.6	1 M $Mn(Ac)_2$ + 1 M $Zn(Ac)_2$ + 2 (4 for posolyte) M KCl + 0.1 M KI	
	50	50[d]				200	32		
	60	25				240	38.4		

a. Cycle number is defined by the number in which the capacity retention is higher than 80%.

b. Volumetric energy density is defined by: Volumetric energy density (Wh L^{-1}) = Volumetric capacity (Ah L^{-1}) * Voltage (V)

c. The volumetric energy density is based on the electrolyte volume in the positive side.

d. Change zinc anode during cycling.

Flow mode is highlighted with blue color.

References

1. X. Zeng, J. Liu, J. Mao, J. Hao, Z. Wang, S. Zhou, C. D. Ling and Z. Guo, *Adv. Energy Mater.*, 2020, **10**, 1904163.
2. C. Xie, T. Li, C. Deng, Y. Song, H. Zhang and X. Li, *Energy Environ. Sci.*, 2020, **13**, 135-143.
3. D. Chao, W. Zhou, C. Ye, Q. Zhang, Y. Chen, L. Gu, K. Davey and S.-Z. Qiao, *Angew. Chem. Int. Ed.*, 2019, **58**, 7823-7828.
4. W. Chen, G. Li, A. Pei, Y. Li, L. Liao, H. Wang, J. Wan, Z. Liang, G. Chen, H. Zhang, J. Wang and Y. Cui, *Nat. Energy*, 2018, **3**, 428-435.
5. G. Liang, F. Mo, H. Li, Z. Tang, Z. Liu, D. Wang, Q. Yang, L. Ma and C. Zhi, *Adv. Energy Mater.*, 2019, **9**, 1901838.
6. J. Huang, Z. Guo, X. Dong, D. Bin, Y. Wang and Y. Xia, *Sci. Bull.*, 2019, **64**, 1780-1787.
7. J. Huang, L. Yan, D. Bin, X. Dong, Y. Wang and Y. Xia, *J. Mater. Chem. A*, 2020, **8**, 5959-5967.
8. D. Chao, C. Ye, F. Xie, W. Zhou, Q. Zhang, Q. Gu, K. Davey, L. Gu and S.-Z. Qiao, *Adv. Mater.*, 2020, **32**, 2001894.
9. C. Liu, X. Chi, Q. Han and Y. Liu, *Adv. Energy Mater.*, 2020, **10**, 1903589.
10. M. Li, Q. He, Z. Li, Q. Li, Y. Zhang, J. Meng, X. Liu, S. Li, B. Wu, L. Chen, Z. Liu, W. Luo, C. Han and L. Mai, *Adv. Energy Mater.*, 2019, **9**, 1901469.
11. G. Li, W. Chen, H. Zhang, Y. Gong, F. Shi, J. Wang, R. Zhang, G. Chen, Y. Jin, T. Wu, Z. Tang and Y. Cui, *Adv. Energy Mater.*, 2020, **10**, 1902085.